Fizika Nizkikh Temperatur, 2005, v. 31, No. 6, p. 629–633

Electrical resistivity of $Ti_{41.5}Zr_{41.5}Ni_{17}$ quasicrystals in the temperature region 0.3–300 K

V.M. Azhazha[1], G.Ya. Khadzhay[2], S.V. Malikhin[3], B.A. Merisov[2], H.R. Ott[4], A.T. Pugachov[3], and A.V. Sologubenko[4]

[1] *National Science Center «Kharkov Institute of Physics and Technology» 1 Academicheskaya Str., Kharkov, 61108, Ukraine*

[2] *Physics Department, Kharkov National University, 4 Svobody Sq., Kharkov, 61077, Ukraine*
E-mail: George.Ya.Khadjai@univer.kharkov.ua

[3] *National Technical University «Kharkov Polytechnical Institute», 21 Frunze Str., Kharkov, Ukraine*

[4] *Laboratorium für Festkörperphysik, ETH Hönggerberg, CH-8093, Zürich, Switzerland*

Received October 20, 2004

The electrical resistivity of icosahedral quasicrystals $Ti_{41.5}Zr_{41.5}Ni_{17}$ was investigated in the temperature region between 0.3 and 300 K on samples of different quality. In the temperature region between 0.3 and 2 K, the influence of external magnetic fields up to 16 kOe on the superconducting transition of these materials was investigated. The temperature dependence of the resistivity in the region of the superconducting transition varies in a step-like manner. The data of the x-ray analysis imply the presence of several different quasicrystalline phases. Above the superconducting transition, a resistivity minimum is observed.

PACS: 61.44.Br, 74.25.Op, **72.15.–v**

1. Introduction

Quasicrystals are a relatively new type of conducting solids with long range order but no periodicity in the crystal structure. The conductivity and especially superconductivity of quasicrystals was not studied in great detail in the past and therefore, new efforts along those lines seem of interest.

The conductivity of quasicrystals is determined by both their electronic structure and by electron-scattering effects [1]. All known quasicrystalline superconductors — Al–Zn–Mg [2]; Al–Cu–Mg, Al–Cu–Li [3]; Ti–Zr–Ni [4,5] — belong to the so-called TC-type, which is characterized by high (in comparison to the MI-type) values of the electron concentration ($e/a \geq 2.1$) and the ratio of the quasicrystallinity parameter to the average atomic diameter ($a_q/d \sim 1.75$) [6]. Regarding the temperature dependence of the electrical resistivity of these TC-type quasicrystals, the derivative $d\rho/dT > 0$ in a broad range of temperature and, in general, the resistivity $\rho \leq 300\ \mu\Omega \cdot$ cm. Thus, in the corresponding temperature region the electrical resistivity of these systems is thus mainly determined by the mean free path of the conduction electrons [1].

In Ref. 5 we reported a low-temperature ($T \approx 20$ K) minimum in the temperature dependence of the resistivity of icosahedral quasicrystalline and superconducting alloys of the Ti–Zr–Ni family. In the present work we report an investigation of the electrical conductivity of alloys of the system Ti–Zr–Ni in a broad temperature range, including a study of the superconducting transition in magnetic fields.

2. Experiment

2.1. Samples

Thin ribbons of quasicrystalline $Ti_{41.5}Zr_{41.5}Ni_{17}$ were obtained by quenching the corresponding liquid on a rapidly rotating copper disk in pure argon atmosphere. As initial elements we used Ti, Zr, Ni of 99.9 purity [4]. The tangential velocity of the disk surface at quenching was v = 19.5 and 25 m/s (samples S19 and S25, respectively). X-ray fluorescence chemical composition control showed less than 0.5% deviation

of the resulting sample composition from the nominal one. The electrical resistivity measurements were done on ribbons with an approximate size of 15×2×(0.02–0.04) mm.

2.2. Measurements

The phase composition of the samples was determined by x-ray diffraction using Cu-K_α and Fe-K_α radiation. The quasicrystalline phase was identified following the method described in Refs. 7–9. Indices for each diffraction peak of the icosahedral structure were attributed following the scheme proposed by J.W. Cahn et al. [7]. According to this scheme, the six-index reflection representation (n_1, n_2, n_3, n_4, n_5, n_6) is replaced, for simplicity, by a two-index variety – (N,M). For characterizing the quasicrystalline structure we used the quasicrystallinity parameter a_q which is related to the module of the diffraction vector, $|\mathbf{Q}|$, as

$$Q = \frac{4\pi \sin\theta}{\lambda} = \frac{\pi}{a_q}\sqrt{\frac{N + M\tau}{2 + \tau}}, \qquad (1)$$

where $\tau = 1.618\ldots$ is the irrational «golden» mean.

The coherence length, L, was estimated from the width of the diffraction lines.

The measurements of the electrical resistivity were done using a standard four-point arrangement. The temperature was measured with ruthenium-oxide thermometers in the interval 0.3–2 K and with rhodium-iron thermometers in the interval 1.5–300 K.

3. Results

3.1. X-ray characteristics of the samples

The x-ray analysis of the samples in a wide range of diffraction angles revealed no admixture of crystalline phases.

A typical feature of the diffraction pictures is the observed asymmetry of the diffraction profiles in the shape of pronounced «tails». For the sample S19, such a «tail» appears at high diffraction angles, but for S25 the «tail» is more pronounced on the small angle side. The asymmetry is more substantial if the profiles are recorded using softer Fe-K_α radiation. The observed diffraction peak intensity distribution is typical for all observed reflections and it can be related to the presence of weak unresolved lines.

In Fig. 1, a part of the typical diffraction pattern taken with Fe-K_α radiation for sample S25 is presented. It includes one of the strongest reflections with the attributed indices (18,29). The separation of diffraction peaks into components was done using a full-profile analysis after a standard treatment involving a background separation and the subtraction of the $K_{\alpha 2}$-doublet. The complex diffraction profile was simulated as a sum of separate peaks described by the Cauchy functions of first and second order. The minimum number of peaks providing the minimum deviation of the summary profiles from the experimental intensity distribution was equal to three for both samples. For each peak, we determined the position, the width and the integral intensity. The results of the signal separation into three components are displayed in Fig. 1.

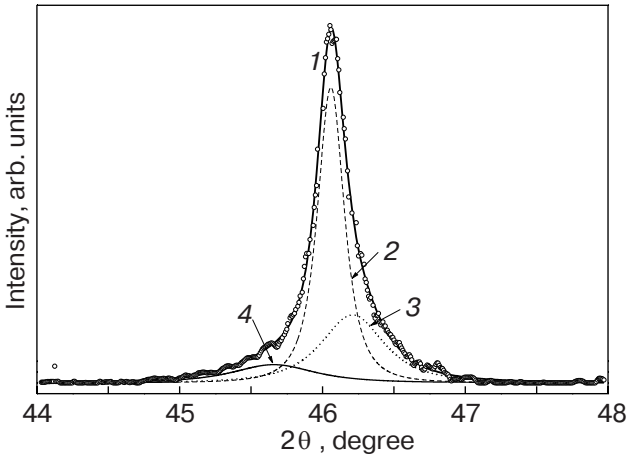

Fig. 1. Experimental distribution of intensity of the diffraction peak (18,29) for sample S25 in λ_{K_α}-Fe radiation (*1*) and the results of a full-profile computer analysis. Curves *2*, *3*, and *4* correspond to the maxima F1, F2, and F3, respectively.

We denote the most intensive (main) peak as P1 and the weak additional peaks as P2 (left) and P3 (right). All additional peaks have the same indices as the main peaks, for all reflections in the spectrum. This implies that the sample contains three quasicrystalline phases with slightly different compositions. It cannot be excluded, however, that one of the phases may be a crystalline approximant W1/1. From the results of the separation, the quasicrystallinity parameter, a_q, and the phase volume portions were determined and shown in Table 1.

Phase P2 (peak F2) is observed in both samples, although there is more of it in S19. The content of phase P3 is significant in S25, while its contribution in S19 is below the limit of experimental uncertainty. The volume portions of phases P2 and P3 are increasing towards the free surface within a subsurface layer of 2–3 μm. The lines of phase P2 are observed near all the main reflections (for example, (18,29), (20,32), (52,84), (136,220)) and give the same value of the parameter a_q. Therefore, we can conclude that this phase is indeed quasicrystalline.

Table 1. Average values of the quasicrystallinity parameter, a_q, the line half-width, B, and the volume portions of different phases in the samples

Phase	S19, v = 19,5 m/s			S25, v = 25 m/s		
	a_q, Å	B, grad.	Volume portion	a_q, Å	B, grad.	Volume portion
P1	5.217	0.22	0.75	5.214	0.13	0.73
P2	5.184	0.33	0.22	5.188	0.32	0.17
P3	5.267	0.49	0.03	5.282	0.36	0.10

As it is seen from Table 1, the volume portions of P1 and P2 as well as the corresponding a_q values are practically equal for both samples. In addition, we note that in sample S25, the line width is smaller and hence, the structural perfection is higher.

3.2. Temperature dependence of the electrical resistivity

The experimental data are presented in Fig. 2. We notice the following features in the temperature dependence of the electrical resistivity for the investigated quasicrystals $Ti_{41.5}Zr_{41.5}Ni_{17}$.

i) Shallow minima in $\rho(T)$ are observed near 20 and 50 K for samples S19 and S25, respectively.

ii) At temperatures above the minima ($T > 20$ K for S19 and $T > 50$ K for S25), a metallic behavior of the resistivity ($d\rho/dT > 0$) is observed. The increase of the resistivity in the temperature range between $T_{\min}$ and 300 K is of the order of 3%.

iii) At temperatures below 1.6 K, onsets of transitions to superconductivity are identified. Zero resistivity was only observed for sample S25 at $T \approx 0.35$ K (Fig. 3,*b*).

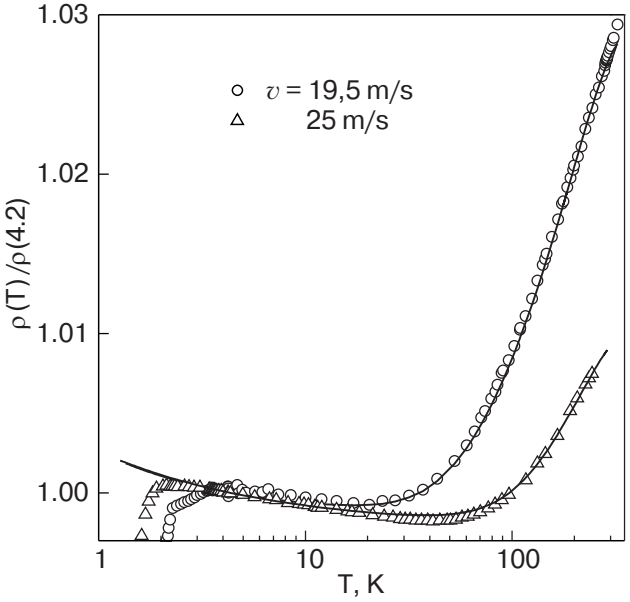

Fig. 2. The temperature dependence of the electrical resistivity of icosahedral quasicrystals $Ti_{41.5}Zr_{41.5}Ni_{17}$. The lines are to guide the eye.

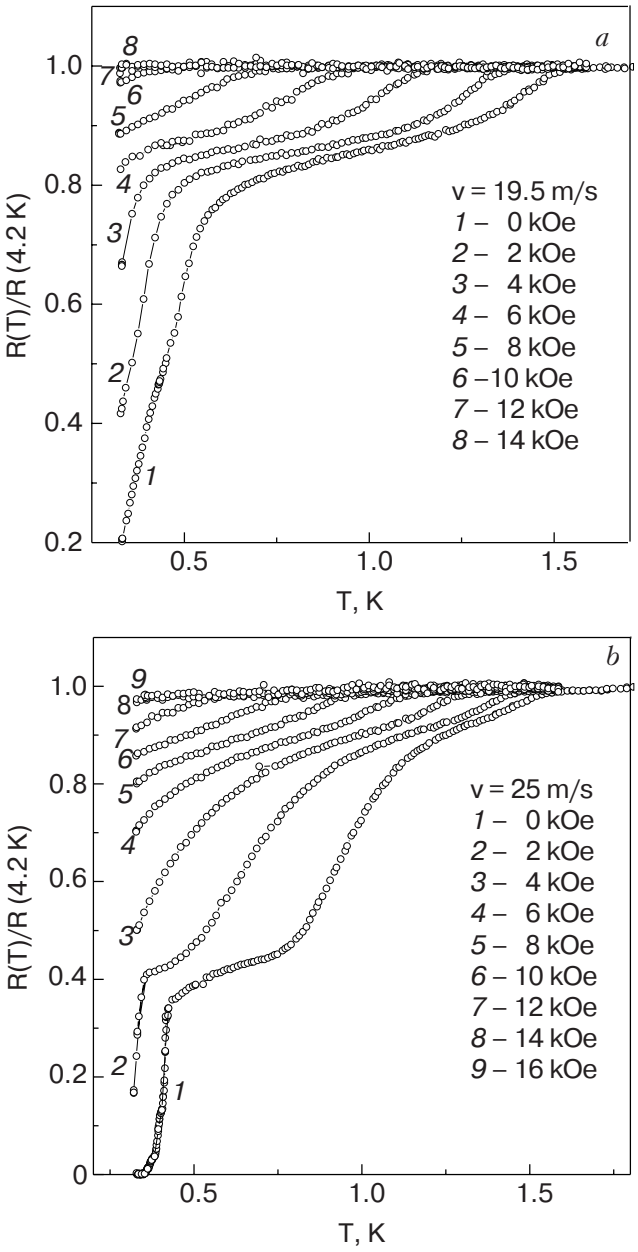

Fig. 3. Electrical resistivity of icosahedral quasicrystals $Ti_{41.5}Zr_{41.5}Ni_{17}$ in magnetic field: S19 (*a*), S25 (*b*).

3.3. The influence of magnetic field on the superconducting transition temperature

In Fig. 3, the transitions to the superconducting state for samples S19 (*a*) and S25 (*b*) in magnetic fields up to 16 kOe are shown. The multistep character of the transitions is most likely caused by inhomogeneities of the samples' phase compositions. The upper limits for the values of the upper critical fields, H_{c2}, were determined from the onset of the deviation of $\rho(T)$ from the normal-state level. The resulting diagrams $H_{c2}(T)$ are presented in Fig. 4.

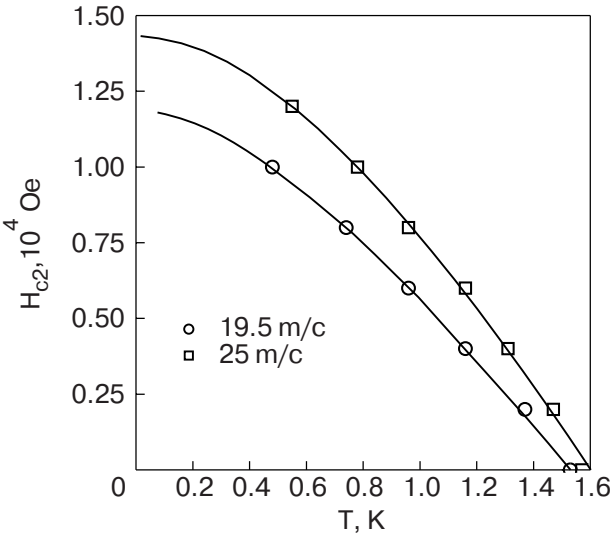

Fig. 4. Temperature dependence of the upper critical field of icosahedral quasicrystals $Ti_{41.5}Zr_{41.5}Ni_{17}$. The lines are to guide the eye.

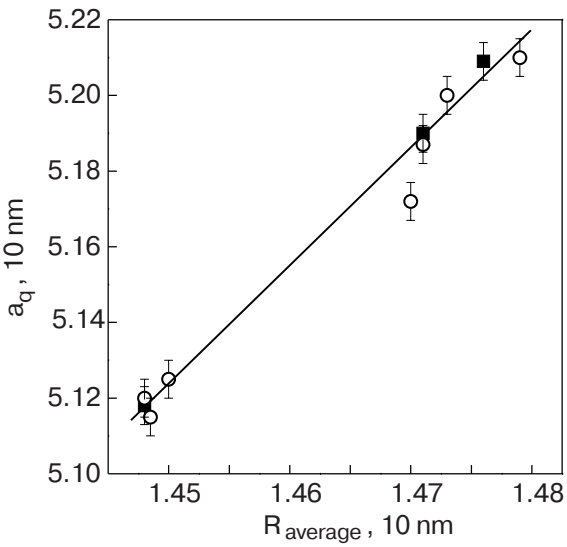

Fig. 5. Quasicrystallinity parameter as a function of the average atomic radius. Solid symbols are own data; open symbols are literature data [3,11,12].

4. Discussion

4.1. The composition of phases

It is known [10] that, in first approximation, the quasicrystallinity parameter is equal to the radius of the Bergman's cluster. This cluster is a structural unit of Ti–Zr–Ni icosahedral quasicrystal. It is clear that its size depends on which kind of atoms and how many of them form the cluster. In Fig. 5, the value a_q as a function of the average atomic radius of the alloy, using our own and literature data [3,11,12] is shown. From this plot one can determine the average atomic radii for phases P1, P2 and P3. Here one has to take into account the following: 1) the dependence in Fig. 5 corresponds to compounds in a rather narrow homogeneity region of the *i*-QC phase and 2) differences in the magnitude of a_q for three phases under consideration cannot be large. Taking into account the above-mentioned arguments, one can practically unambiguously identify the composition of the phases with an accuracy of ~0.5 at.%. The reliability criterion for the selection is the coincidence of the nominal $Ti_{41.5}Zr_{41.5}Ni_{17}$ sample composition with the value calculated by adding up the three identified phases with their volume portions. The best agreement is obtained if the phases have the following compositions: P1 — $Ti_{40}Zr_{42.5}Ni_{17.5}$, P2 — $Ti_{40}Zr_{40}Ni_{20}$ and P3 — $Ti_{43.5}Zr_{43.5}Ni_{13}$.

Note that, according to the equilibrium diagram for Ti–Zr–Ni system, the phase compositions P1 and P2 are in the stability region of the quasicrystalline phase. The phase P3 composition lies within the existence region of 1/1 approximant [13, 14].

4.2. The superconducting transition

The multi-step behavior of $\rho(T)$ at low temperatures, which is observed for both samples, is consistent with the data of the x-ray phase analysis. In zero magnetic field there are three steps in the resistivity drop for sample S25, which we interpret as superconducting transitions in each phase. For S19, only two such steps are observed because one of the phases (P3) is practically absent in this specimen (Fig. 3). It is difficult to ascribe each $\rho(T)$ step to a particular phase because of the complex interconnection between regions of various size and different phases and the associated proximity effect. However, since the resistivity reaches zero only for sample S25 at $T < 0.4$ K (Fig. 3,*b*), it is plausible that it is phase P1 which is the main component of this sample that is responsible for the relatively sharp step in the region $T < 0.4$ K, leading to the zero resistivity. Because in sample S19 the phase structure is less perfect than in S25, the superconducting transition for the P1 phase in S19 is broader, and in the covered temperature range ($T > 0.3$ K), zero resistance is not achieved.

The broader superconducting transitions in phases P1 and P2 seem to lead to the step-like features in the temperature dependence of the electrical resistivity.

4.3. The temperature dependence of the upper critical field

In Fig. 4, the temperature dependences of the upper critical field $H_{c2}(T)$ are shown for phase P2 which has the maximum superconducting critical temperature in both samples. One can see that $H_{c2}(T)$ is higher for

the structurally more perfect sample S25. Our data are qualitatively similar to the H_{c2}(T) curves for icosahedral quasicrystals Al–Cu–Li and Al–Cu–Mg, obtained in [3]. However, the critical fields at low temperatures for quasicrystals of system Ti–Zr–Ni are considerably higher than those for Al–Cu–Li and Al–Cu–Mg, in spite of similar values of T_c between 0.8 and 1.5 K of these alloys [3].

4.4. The temperature dependence of resistivity

The minima in $\rho(T)$ may be caused by the influence of weak localization of electrons at low temperatures [6]. Above T_{min}, the temperature variation of the resistivity is close to $\rho(T) \propto T^3$. For metallic systems this is usually related to electron-phonon *s–d* scattering, although in our case its contribution to the total resistivity is largely masked by much stronger scatterings caused by the structural disorder, the electron-electron interaction, and the localization effects. We note that for sample S25 which appears to be structurally more perfect, the resistivity minimum appears at a distinctly higher temperature ($T_{min} \approx 50$ K) than for the less perfect sample S19 ($T_{min} \approx 20$ K).

5. Conclusions

We investigated the phase composition, the structure and the temperature dependence of electrical resistivity of icosahedral quasicrystals of nominal composition $Ti_{41.5}Zr_{41.5}Ni_{17}$ in the region 0.3–300 K. In the region 0.3–1.6 K, the influence of magnetic fields up to 16 kOe on the superconducting transition was investigated.

The x-ray analysis revealed the existence of three phases with almost equal chemical composition, two of which are icosahedral and the third phase can be associated with the 1/1-approximant. The volume concentration of the phases was estimated, and the superconducting temperatures were determined.

The upper critical field obtained for the phase with the highest T_c is higher for the structurally more perfect sample.

The temperature dependence of the resistivity in the region between T_c and T_{min} is probably determined by effects of weak localization of conduction electrons. At $T > T_{min}$, the influence of the scattering of electrons by phonons is also observed. The resistivity minimum for the more perfect sample is shifted to higher temperatures in comparison to the less-perfect sample.

This work was supported by Swiss National Science Foundation in ranges of Joint Research Project Nr. 7UKPJ062171.

1. U. Mizutani, *Materials Science and Engineering* **294–296**, 464 (2000).
2. J.F. Graebner and H.S. Chen, *Phys. Rev. Lett.* **58**, 1945 (1987).
3. J.L. Wagner, B.D. Bigs, K.M. Wong, and S.J. Poon, *Phys. Rev. Lett.* **B38**, 7436 (1988).
4. V. Azhazha, A. Grib, G. Khadzhay, S. Malikhin, B. Merisov, and A. Pugachov, *Phys. Lett.* **A303**, 87 (2002).
5. V. Azhazha, G. Khadzhay, S. Malikhin, B. Merisov, and A. Pugachov, *Phys. Lett.* **A349**, 539 (2003).
6. *Physical Properties of Quasicrystals*, Z.M. Stadnik (ed.), Springer, Berlin (1999).
7. J.W. Cahn, D. Shechtman, and D. Gratias, *J. Mater. Res.* **1**, 13 (1986).
8. S. Ebalard and F. Spaepen, *J. Mater. Res.* **4**, 39 (1989).
9. P.J. Lu, K. Deffeyes, P.J. Steinhardt, and N. Yao, *Phys. Rev. Lett.* **87**, 275507-1 (2001).
10. V. Azhazha, S. Dub, G. Khadzhay, B. Merisov, S. Malykhin, and A. Pugachov, *Philos. Mag.* **84**, 983 (2004).
11. A.M. Viano, E.H. Majzoub, R.M. Stroud, M.J. Kramer, S.T. Misture, P.C. Gibbons, and K.F. Kelton, *Philos. Mag.* **A78**, 131 (1998).
12. R. Nicula, A. Jianu, and A.R. Biris, *Europhys. J.* **B3**, 1 (1998).
13. I. Davis, E. Majzoub, J. Simmons, and K. Kelton, *Materials Science and Engineering* **296**, 104 (2000).
14. K.F. Kelton, A.K. Gangopadhyay, G.W. Lee, L. Hannet, R. W. Hyers, S. Krishnan, M.B. Robinson, J. Rogers, and T.J. Rathz, *J. Cryst. Solids* **312–314**, 305 (2002).